

# Tug-of-War in a Double-Nanopore System

Aniket Bhattacharya\* and Swarnadeep Seth

Department of Physics, University of Central Florida, Orlando, Florida 32816-2385, USA

(Dated: April 24, 2022)

We simulate a tug-of-war (TOW) scenario for a model double-stranded DNA threading through a double nanopore (DNP) system. The DNA, simultaneously captured at both pores is subject to two equal and opposite forces  $-\vec{f}_L = \vec{f}_R$  (TOW), where  $\vec{f}_L$  and  $\vec{f}_R$  are the forces applied to the left and the right pore respectively. Even though the net force on the DNA polymer  $\Delta\vec{f}_{LR} = \vec{f}_L + \vec{f}_R = 0$ , the mean first passage time (MFPT)  $\langle\tau\rangle$  depends on the magnitude of the TOW forces  $|f_L| = |f_R| = f_{LR}$ . We qualitatively explain this dependence of  $\langle\tau\rangle$  on  $f_{LR}$  from the known results for the single-pore translocation of a triblock copolymer A-B-A with  $\ell_{pB} > \ell_{pA}$ , where  $\ell_{pA}$  and  $\ell_{pB}$  are the persistence length of the A and B segments respectively. We demonstrate that the time of flight (TOF) of a monomer with index  $m$  ( $\langle\tau_{LR}(m)\rangle$ ) from one pore to the other exhibits quasi-periodic structure commensurate with the distance between the pores  $d_{LR}$ . Finally, we study the situation where we offset the TOW biases so that  $\Delta\vec{f}_{LR} = \vec{f}_L + \vec{f}_R \neq 0$ , and qualitatively reproduce the experimental result of the dependence of the MFPT on  $\Delta f_{LR}$ . We demonstrate that for a moderate bias, the MFPT for the DNP system for a chain length  $N$  follows the same scaling ansatz as that of for the single nanopore,  $\langle\tau\rangle = (AN^{1+\nu} + \eta_{pore}N)(\Delta f_{LR})^{-1}$ , where  $\eta_{pore}$  is the pore friction, which enables us to estimate  $\langle\tau\rangle$  for a long chain. Our Brownian dynamics simulation studies provide fundamental insights and valuable information about the details of the translocation speed obtained from  $\langle\tau_{LR}(m)\rangle$ , and accuracy of the translation of the data obtained in the time-domain to units of genomic distances.

PACS numbers:

## I. INTRODUCTION

Nanopore (NP) sensing is a powerful approach for accurate, fast and cost-effective detections of biomolecules, such as single and double stranded DNA, peptides and proteins [1]. For almost two decades, research in this area has spurred continued and increased activities among broad disciplines of sciences and engineering due to their direct impact on human health and diseases. Unlike traditional methods, which require molecular amplification, in a single NP (SNP) based method [2], a particular DNA segment is analyzed as the nucleotides make single file translocation through the NP. Since its original demonstration in  $\alpha$ -hemolysin protein pore [3–6], NP translocation has been studied in other biological NPs, nanopores in silicon nitride membranes, and two dimensional (2D) materials, such multi-layered graphene NPs. Recently translocation of a DNA segment has been extended in double-NP systems after being co-captured by both the pores [7–11]. Compared to a single NP, double, or multiple NPs detection methods with adjustable bias and feedback applied at each pore offer better control of the DNA. Different variations of this concept, such as DNP separated by a nano-bridge [12], double-barrel NP [13], nanoscale pre-confinement [14], and entropy driven TOW [15] have also been reported.

While translocation through a single NP has been studied quite extensively theoretically, experimentally, and

using a variety of numerical and simulation strategies, theoretical studies and modeling translocation in double or multiple NP system is only directed to explain a specific experimental system [7].

In this paper, we report Brownian dynamics (BD) simulation studies of a coarse-grained (CG) model homopolymer translocating through a DNP system. Our model DNP system *in silico* is a simplified version of the experimental designs of DNP systems reported recently [8, 9] in which we study the effects of chain stiffness  $\kappa$ , distance between the pores  $d_{LR}$ , the magnitude of the biases  $\vec{f}_L$  and  $\vec{f}_R$  on the MFPT  $\langle\tau\rangle$ , and on the TOF of the individual monomers to provide further details of various aspects of translocation through a DNP. The CG model as described in the next section does not require detail structures of the DNA and is sufficient to answer the questions addressed in this paper. We have chosen  $d_{LR} \ll L$ , the contour length of the chain. and often used the known results from scaling theory of polymer translocation [16, 17, 19], nonequilibrium tension propagation (TP) theory of polymer translocation [20], and prior results for SNP translocation for a stiff chain [21] to explain the results for DNP translocation in this limit. These studies provide information to design new experiments with different parameter sets, develop a theoretical framework that can be tested by additional simulation studies.

## II. MODEL

Our BD scheme is implemented on a bead-spring model of a polymer with the monomers interacting via

\*Author to whom the correspondence should be addressed; Electronic address: AniketBhattacharya@ucf.edu

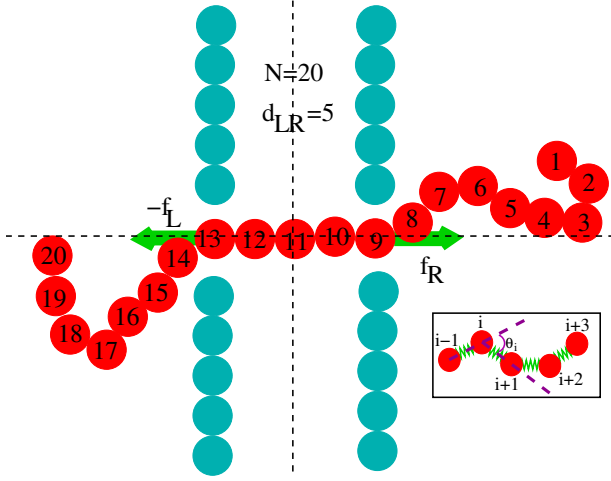


FIG. 1: Schematic of BD simulation model for a chain of length  $N = 20$  (red). Initial configuration of the chain between the pores  $d_{LR}$  apart is approximately a straight line. The immobilized walls on which the two pores are located are created by particles (teal) of the same diameter. External biases  $\vec{f}_L$  and  $\vec{f}_R$  are applied in each pore in opposite directions as shown. The box shows the details of the bead-spring model. The local persistence length  $\ell_p(i) = -1/\ln\langle\cos\theta_i\rangle$  is calculated from the angle  $\theta_i$  (Eqn. 7)

an excluded volume (EV), a Finite Extension Nonlinear Elastic (FENE) spring potential, and a bond-bending potential enabling variation of the chain persistence length  $\ell_p$  (Fig. 1). The model, originally introduced for a fully flexible chain by Grest and Kremer [22], has been studied quite extensively by many groups using both Monte Carlo (MC) and various molecular dynamics (MD) methods [23]. Recently we have generalized the model for a semi-flexible chain and studied both equilibrium and dynamic properties [21, 24]. Comparison of our BD results with those obtained for very large self-avoiding chains on a square lattice reveals robustness of the model for certain universal aspects, e.g., scaling of end-to-end distance and transverse fluctuations [24–27]. Using our BD scheme for confined stiff polymers in nanochannels we have demonstrated and verified the existence of Odijk deflection length  $\lambda \sim (\ell_p D^2)^{1/3}$  [27]. More recently we compared the evolution of the density profile along the nanochannel axis obtained from the BD simulation with those obtained from an approach using Nonlinear Partial differential equation [28] with excellent agreement showing the applicability of the BD simulation method to study nonequilibrium dynamics of confined polymers. The BD simulation provides detailed picture of how a stiff chain folds into a series of nested loops when pushed by a nanodozer [29]. Last but not the least we have used the same model earlier to address various problems in SNP translocation with success [30–33]. The successes of these prior studies explaining a variety of phenomena provide assurance that the BD simulation studies will

provide useful informations and insights toward a fundamental understanding of polymer translocation through a model DNP system.

The EV interaction between any two monomers is given by a short range Lennard-Jones (LJ) potential

$$U_{LJ}(r) = 4\epsilon \left[ \left( \frac{\sigma}{r} \right)^{12} - \left( \frac{\sigma}{r} \right)^6 \right] + \epsilon, \text{ for } r \leq 2^{1/6}\sigma; \\ = 0, \text{ for } r > 2^{1/6}\sigma. \quad (1)$$

Here,  $\sigma$  is the effective diameter of a monomer, and  $\epsilon$  is the strength of the LJ potential. The connectivity between neighboring monomers is modeled as a FENE spring with

$$U_{FENE}(r) = -\frac{1}{2}k_F R_0^2 \ln(1 - r_{ij}^2/R_0^2). \quad (2)$$

Here  $r_{ij} = |\vec{r}_i - \vec{r}_j|$  is the distance between the consecutive monomer beads  $i$  and  $j = i \pm 1$  at  $\vec{r}_i$  and  $\vec{r}_j$ ,  $k_F$  is the spring constant and  $R_0$  is the maximum allowed separation between connected monomers. The chain stiffness  $\kappa$  is introduced by adding an angle dependent three body interaction term between successive bonds as (Fig. 1)

$$U_{\text{bend}}(\theta_i) = \kappa(1 - \cos\theta_i) \quad (3)$$

Here  $\theta_i$  is the angle between the bond vectors  $\vec{b}_{i-1} = \vec{r}_i - \vec{r}_{i-1}$  and  $\vec{b}_i = \vec{r}_{i+1} - \vec{r}_i$ , respectively, as shown in Fig. 1. The strength of the interaction is characterized by the bending rigidity  $\kappa$  associated with the  $i^{\text{th}}$  angle  $\theta_i$ . For a homopolymer chain the bulk persistence length  $\ell_p$  of the chain in two dimensions (2D) is given by [34]

$$\ell_p/\sigma = 2\kappa/k_B T. \quad (4)$$

Each of the two purely repulsive walls consists of one mono-layer (line) of immobile LJ particles of the same diameter  $\sigma$  of the polymer beads symmetrically placed at  $\pm \frac{1}{2}d_{LR}$ . The two nanopores are created by removing two particles at the center of each wall. We use the Langevin dynamics with the following equations of motion for the  $i^{\text{th}}$  monomer

$$m\ddot{\vec{r}}_i = -\nabla(U_{LJ} + U_{FENE} + U_{\text{bend}} + U_{\text{wall}}) - \Gamma\dot{\vec{v}}_i + \vec{\eta}_i. \quad (5)$$

Here  $\vec{\eta}_i(t)$  is a Gaussian white noise with zero mean at temperature  $T$ , and satisfies the fluctuation-dissipation relation in  $d$  physical dimensions (here  $d = 2$ ):

$$\langle \vec{\eta}_i(t) \cdot \vec{\eta}_j(t') \rangle = 2dk_B T \delta_{ij} \delta(t - t'). \quad (6)$$

We express length and energy in units of  $\sigma$  and  $\epsilon$ , respectively. The stiffness parameter  $\kappa$  is expressed in units of  $\epsilon$ , and the parameters for the FENE potential in Eq. (2),  $k_F$  and  $R_0$ , are set to  $k_F = 30\epsilon/\sigma$  and  $R_0 = 1.5\sigma$ , respectively. The friction coefficient and the temperature are set to  $\Gamma = 0.7\sqrt{m\epsilon/\sigma^2}$ ,  $k_B T/\epsilon = 1.2$ , respectively. The force is measured in units of  $k_B T/\sigma$ . The numerical integration of Equation (5) is implemented using the algorithm introduced by Gunsteren and Berendsen [35]. Our

previous experiences with BD simulation suggests that for a time step  $\Delta t = 0.01$  these parameters values produce stable trajectories over a very long period of time and do not lead to unphysical crossing of a bond by a monomer [26, 27]. The average bond length stabilizes at  $b_l = 0.971 \pm 0.001$  with negligible fluctuation regardless of the chain size and rigidity [26]. We have used a Verlet neighbor list [36] instead of a link-cell list to expedite the computation.

### III. SIMULATION RESULTS

We carried out simulations for chain lengths  $N = L/\sigma = 64, 96, 128, 192, 256, 320$ , and 384 (where  $L$  is the corresponding chain contour length) for various chain stiffness  $\kappa = 0, 16, 32, 64$ , as well as for several distances between the pores  $d_{LR}$  for consistency checks, but show only limited set of results  $d_{LR}/\sigma = 16$  and 32 and mostly for  $\kappa = 8$  and 16. The simulation results are averaged over at least 2000 initial conditions. For exact tug-of-war situation and for small biases the computations can be prohibitively large compared to even a weakly biased situation.

The starting point of our study is a homopolymer already co-captured by both the pores and placed symmetrically with the number of beads at the left side of the left pore ( $n_L$ ) and at the right side of the right pore ( $n_R$ ) are the same (Fig. 1), so that  $n_L + n_R + n_m = 2n_L + n_m = N$ , where  $n_m$  represents the number of monomers in between the two pores. Our initial configuration is a straight chain with  $d_{LR} = n_m\sigma$ , which is then equilibrated with BD simulation time about 5 times the Rouse relaxation time  $\tau_{eq} \propto N^{1+2\nu}$  keeping the two beads, located inside the left and the right pore clamped, where  $\nu = 0.75$  is the Flory exponent in two dimensions [37]. In simulation the local chain persistence length is calculated from  $\langle \cos \theta_m \rangle$  via

$$\ell_p(m) = -\ln \frac{1}{\langle \cos \theta_m \rangle}, \quad (7)$$

where  $m$  is the monomer index. Previously we have checked that the two definitions (Eqns. 4 and 7) become equivalent for a free homopolymer chain and that for a heteropolymer chain, the calculation of the  $\langle \cos \theta_i \rangle$  provides the correct way to determine the local chain persistence length [24]. After the polymer chain is equilibrated with beads inside the left and right pores at the clamped positions, the chain is allowed to translocate with biases applied at the left and the right pores as shown in Fig. 1. We consider both the cases  $\vec{f}_L + \vec{f}_R = 0$  and  $\vec{f}_L + \vec{f}_R \neq 0$ .

#### A. TOW - local chain persistence length $\ell_p(m)$

First we study the TOW situation where the chain is subject to two equal and opposite forces  $\vec{f}_L$  and  $\vec{f}_R$  (Fig. 1) at the left and right pores. Since the net force is

zero, the chain executes diffusive motion until it translocates (exits) either through the left or through the right pore. However, unlike an unbiased translocation in a SNP, the persistence length of the chain segment in between the two pores becomes larger due to the presence of TOW forces. This causes the effective local persistence length to be a function of the monomer index  $m$ , so that the average effective persistence length of the entire chain becomes larger as shown in Fig. 2. We observe that the effect is most prominent for  $\kappa = 0$  (Fig. 2(a)), which will be relevant if similar experiments are performed for a single stranded DNA. Figs. 2(a)-(c) for  $\kappa = 0, 16$ , and 64 look qualitatively similar, however, the scales are very different. Evidently, the effect is less pronounced for a stiffer chain as the relative increase in the chain persistence length is less for the same TOW forces  $f_{LR}$ .

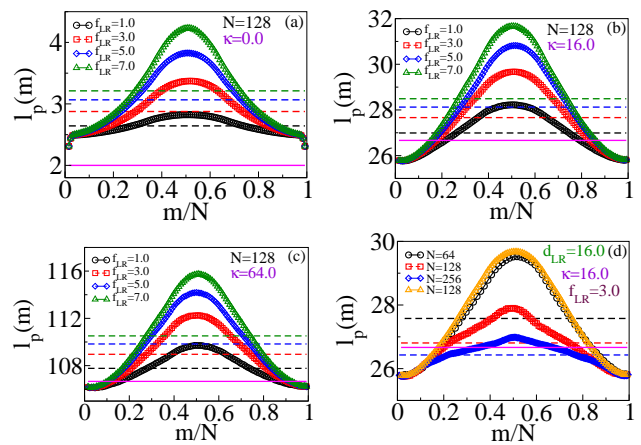


FIG. 2: The local chain persistence length  $\ell_p(m)$  as a function of reduced monomer index  $m/N$ . (a) for  $\kappa = 0.0$ , (b)  $\kappa = 16.0$ , and (c)  $\kappa = 64.0$ . The black circles, red squares, blue diamonds, and green triangles correspond to TOW bias  $f_{LR} = 1, 3, 5$ , and 7 respectively. Fig. (d) shows the effect of an increase in chain length  $N$ ; black circles, red squares, and blue diamonds are for  $N = 64, 128$ , and 256 respectively. The orange triangles and the black squares compare a case where  $d_{LR}/N = 16/64 = 32/128 = \frac{1}{4}$  for two chain lengths. Each dashed line is the average  $\ell_p$  for the same color. In (a)-(c), the solid purple line represents  $\ell_{p0} = 2\kappa/k_B T$  for the unconstrained chain.

#### B. Tug-of-war and MFPT

One then wonders how does this variation in chain persistence length affect the MFPT? Fig. 3(a) shows the variation of MFPT as a function of the TOW forces  $f_{LR}$ . Consistence with Fig. 2 we observe a noticeable increase in  $\langle \tau \rangle$  for  $\kappa = 0$ , and a relatively small increment for chains with  $\kappa = 16$  and 64. The result can be understood from a prior result for the single pore translocation [21], where it has been shown that the  $\langle \tau \rangle$  increases with increasing chain stiffness  $\kappa$ . For the DNP, the TOW forces make the chain segment between the pores stiffer.

The relative degree of increase in persistence length depends on the original stiffness  $\kappa$  of the chain, measured in terms of the ratio  $(\ell_p(N/2) - \ell_p(1))/\langle \ell_p \rangle$  is about 80%, 20%, and 7% for  $\kappa = 0, 16$  and  $64$  respectively. This explains why for the same set of  $f_{LR}$ , the relative increase in chain stiffness for the segment in between the pores is less significant for  $\kappa = 16$  and  $64$ , compared to  $\kappa = 0$ . It is worthwhile to note that for longer chains when  $d_{LR}/L \rightarrow 0$ , the entropic forces of the free segments on either side of the pores become the dominant forces. Thus, it is conceivable that the tiny slope (Fig. 3(a)) observed for  $\kappa = 16$  and  $64$  of the TOW for chains of size  $N = 128$  is a finite size effect. For longer chains  $\langle \tau \rangle$  will have no dependence on the TOW forces  $f_{LR}$ .

### C. TOW and a model triblock copolymer A-B-A

We validate our interpretation by performing a separate set of simulation. We set  $f_L = f_R = 0$  and study the translocation of a triblock copolymer of the form (*flexible-stiff-flexible*) such that  $2n_A + n_B = N$ , and  $n_B\sigma = d_{LR}$ , where  $n_A$  and  $n_B$  are the length segments of the A and B segments respectively. We choose the chain stiffness  $\kappa_B > \kappa_A$ . Keeping  $\kappa_A$  constant we calculate the MFPT as an increasing function of  $\kappa_B$ . As expected, the translocation time increases as a function of the chain stiffness  $\kappa_B$  (Fig. 3(b)). We should mention that analogy is valid on an average. The difference with the A-B-A copolymer and the a homopolymer subject to a TOW is that in the former case, the persistence lengths along the chain are fixed, while for the TOW, it is depends on the location of the chain segment with respect to the two pores. A translocating segment will have an increased persistence length while residing in the region in between the pores. Thus on an average, in a TOW situation, the magnitude of equal and opposite biases at each pore location affects the translocation time for a homopolymer chain. (Fig. 3(b)). The dependence of MFPT on  $\Delta \tilde{f}_{LR}$  will be relevant for experiments done with a single stranded DNA (ssDNA).

### D. TOW and the TOF $\langle \tau_{LR}(m) \rangle$

BD simulation provides detail information about the segmental translocation process. One of the key questions in a TOW situation is how long does a monomer with index  $m$  take to cross the region in between the pores during the translocation (denoted as  $\langle \tau_{LR}(m) \rangle$ )? Experimentally this quantity is measured repeatedly in a DNA flossing experiment [10]. The TOF  $\langle \tau_{LR}(m) \rangle$  should be contrasted with the MFPT  $\langle \tau \rangle$ , which is the average total time of translocation for the entire chain. Since the TOF  $\langle \tau_{LR}(m) \rangle$  can be measured experimentally [9, 10], it can provide further informations. The dependence of

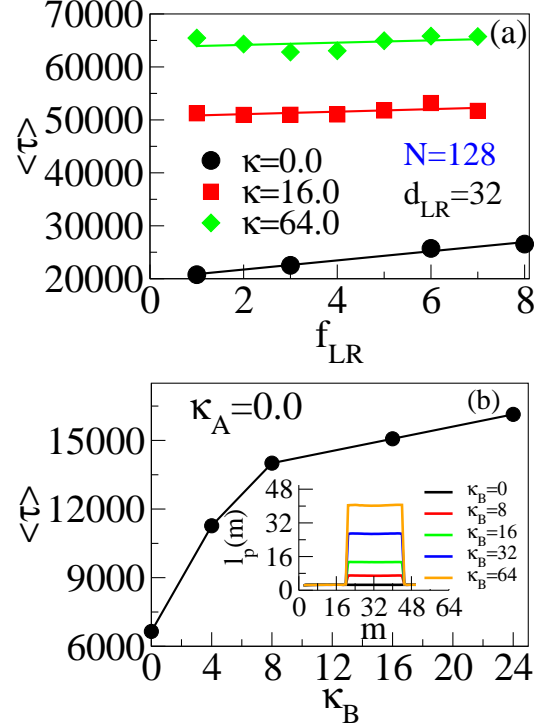


FIG. 3: (a) MFPT as a function of TOW forces  $f_{LR}$  for  $\kappa = 0$  (black circles),  $\kappa = 16$  (red squares), and  $\kappa = 64$  (green diamonds). The straight lines through the points are least square fits through the simulation data. (b) MFPT for a triblock copolymer chains A-B-A ( $\kappa_A = 0.0$ ) as a function of  $\kappa_B$ . The inset shows the corresponding  $\ell_p(m)$  for  $\kappa_B = 0, 8, 16, 32$ , and  $64$  respectively.

the normalized TOF defined as

$$\langle \tilde{\tau}_{LR}(m) \rangle = \frac{\langle \tau_{LR}(m) \rangle}{\langle \tau_{LR} \rangle} \quad (8)$$

on  $f_{LR}$  and  $d_{LR}$  is shown in Fig. 4, where

$$\langle \tau_{LR} \rangle = \sum_m \langle \tau_{LR}(m) \rangle. \quad (9)$$

Please note that the plot is made symmetric by combining the data from the left and right translocation (we checked that the data looks statistically similar with 50% translocation from left to right and *vice-versa*). In experiments [8, 9], the ratio  $d_{LR}/L \ll 1$ . We also show some results for  $d_{LR}/L = 0.25$  to understand the limit  $d_{LR}/L \ll 1$  better.

Fig. 4(a) show significant variations in  $\langle \tilde{\tau}_{LR}(m) \rangle$ . The almost linear decrease for  $m/N \geq 0.75$  (or rise  $m/N < 0.25$ ) corresponds to the last/first 32 (25%) monomers exiting through the right/left pore when they are subject to only one of the TOW forces. The monomers  $m \simeq N/2$  can have a nonzero  $\langle \tilde{\tau}_{LR}(m) \rangle$  if they first travel either to the left/right pore and, then finally exit. Thus the  $\langle \tilde{\tau}_{LR}(m) \rangle$  is minimum at  $m = N/2$ . The monomers which follow the central

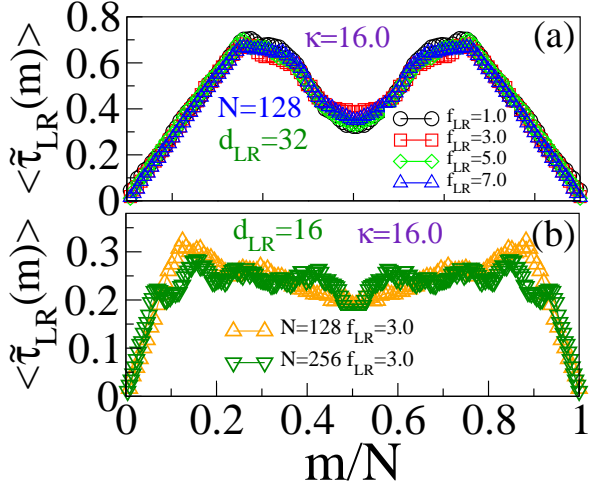


FIG. 4: The normalized TOF  $\langle \tilde{\tau}_{LR}(m) \rangle$  as a function of the reduced monomer index  $m/N$ . (a) The top curves are for  $N = 128$  for four different magnitudes of the TOW forces  $f_{LR} = 1$  (black circles),  $f_{LR} = 3$  (red squares) and green diamonds ( $f_{LR} = 3$ ), and  $f_{LR} = 7$  (blue triangles) respectively. (b). The bottom two curves are for  $d_{LR} = 16$  for chain lengths  $N = 128$  (yellow triangles) and  $N = 256$  (green triangles) respectively.

monomer has to have an increased  $\langle \tilde{\tau}_{LR}(m) \rangle$  until  $m/N \simeq d_{LR}/N\sigma$ . This explains the shape of the four  $\langle \tilde{\tau}_{LR}(m) \rangle$  for  $d_{LR}/L = 32/128 = 1/4$  in Fig. 4(a). One observes that the shape of the  $\langle \tilde{\tau}_{LR}(m) \rangle$  is independent of the magnitude of the TOW force  $f_{LR}$  provided that the value of the chain stiffness is high enough compared to other parameters of the system.

What happens in the limit  $d_{LR}/L \rightarrow 0$ ? The experiments are done in this limit. This limit can be predicted from the shape of the two curves of Fig. 4(b). Here we plot the corresponding  $\langle \tilde{\tau}_{LR}(m) \rangle$  for  $d_{LR}/L = 16/128 = 0.125$  and  $d_{LR}/L = 16/256 = 0.0625$  so that  $d_{LR} \ll L$ . We notice similar feature at the end and at the center. However, for  $N = 256$  we observe a reasonably flat  $\langle \tilde{\tau}_{LR}(m) \rangle$ , albeit with a small amplitude periodic oscillation in units of  $d_{LR}/L$  for monomers satisfying  $0.5d_{LR}/L \leq m/N < (L - d_{LR})/L$ . This we believe is due to different environment a monomer encounters as it enters from the region located at the left side of the left pore  $\rightarrow$  the region in between the pores  $\rightarrow$  the region located at the right side of the right pore of width  $d_{LR} \simeq m\sigma$ . The fine structure of the  $\langle \tilde{\tau}_{LR}(m) \rangle$  can possibly be detected from DNA flossing experiments reported recently [10], where the current blockade due to a known genomic length segment tagged by proteins is measured repeatedly by altering the bias between the pores.

### E. Translocation with a net bias

In a TOW situation, the translocation process is diffusive and hence slow. Thus a more desirable situation is to apply a net, albeit a small bias  $\Delta f_{LR} = \vec{f}_L + \vec{f}_R \neq 0$  so that the DNA can move slowly. The presence of two forces at each pore can provide a feedback mechanism to control the movement of the translocating chain [9]. We define  $\Delta f_{LR} = \pm |\Delta f_{LR}|$ , where the  $\pm$  sign refers to direction of the net force  $\vec{f}_{LR}$  (positive/negative for left/right to right/left translocation). We observe that for a low bias ( $|\Delta f_{LR}| < k_B T/\sigma$ ), the MFPT initially decreases almost exponentially (Fig. 5), and when the bias is increased beyond  $|\Delta f_{LR}|\sigma \geq k_B T$ , then the MFPT decays with a power law  $\langle \tau \rangle \sim |\Delta f_{LR}|^{-1}$ . The shape of the curve from our simulation (Fig. 5) is almost the same as reported in DNP experiment by Zhang *et al.* [9]. Since the length and time scale of simulation and experimental scales are different, it seems that this behavior is generic, independent of the size of the system. The inset

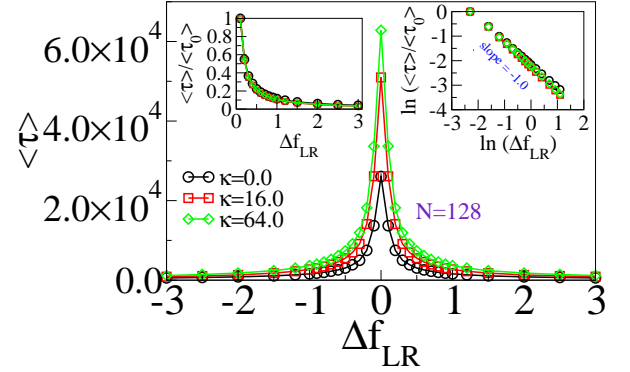


FIG. 5: MFPT as a function of  $\Delta f_{LR}$ . The black, red, green, and blue lines refer to chain stiffness  $\kappa = 0, 16$ , and  $64$  respectively. The inset at the left shows normalized MFPT where all the plots collapse onto the same master plot. The inset at the right is the corresponding plot of the inset at left on a logarithmic scale.

of Fig. 5 at the left shows the normalized  $\langle \tau \rangle / \langle \tau_0 \rangle$  for several values of  $\kappa$ , demonstrating that this is a generic feature for a wide range of chain stiffness. Here we have chosen the normalization factor  $\langle \tau_0 \rangle$  to be the MFPT for  $\Delta f_{LR} = 0.1$ . This eliminates the chain length dependence of  $\langle \tau \rangle$ . The inset Fig. 5 at the right shows that the  $\langle \tau \rangle \sim |\Delta f_{LR}|^{-1}$  (for  $1.0 < \Delta f_{LR} \leq 3$ ) [21]. We have checked that for  $d_{LR} = 16$  and  $24$  and for chain length  $N = 64 - 256$  that this trend is the same. Similar dependence on the force has been observed for SNP translocation [21].

We complete our scaling analysis by studying the chain length dependence of the MFPT. We find that  $\langle \tau \rangle \sim N^{1.5}$  as evident from (i) the data collapse of the histogram of the MFPT and the (ii) two insets of Fig. 6. The slope for each curve at the inset at the right for  $\Delta f_{LR} = 1, 2, 3$  is  $1.5 \pm 0.02$ . Fig. 6 shows this data collapse. Furthermore,

combining these results with  $\langle \tau \rangle \sim |\Delta f_{LR}|^{-1}$  we obtain

$$\langle \tau \rangle = A |\Delta f_{LR}|^{-1} N^{1.5} \quad (10)$$

The inset at the left of Fig. 6 convincingly shows the data collapse for two chain lengths  $N = 128$  and  $256$  for two values of  $\Delta f_{LR} = 2$  and  $3$  respectively, verifying Eqn. 10. This power law scaling of Eqn. 10 with the value

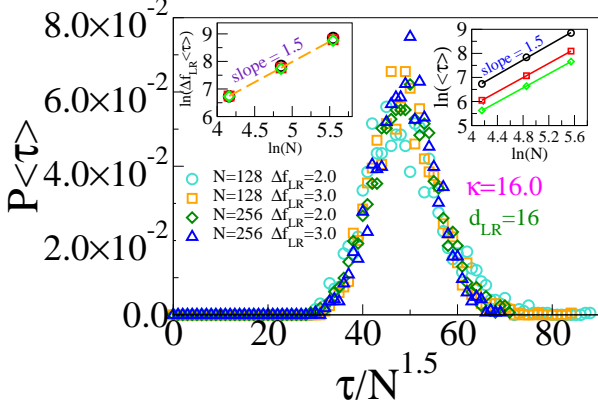


FIG. 6: Histogram of the MFPT as a function of  $\tau/N^{1.5}$  for two different net bias  $\Delta f_{LR}$  and two chain length  $N = 128$  and  $256$  which shows data collapse; Teal circles and orange squares correspond to  $N = 128$  and  $\Delta f_{LR} = 2$  and  $3$ . Green diamonds and blue circles correspond to  $N = 256$  and  $\Delta f_{LR} = 2$  and  $3$ . The inset at the right shows plots for  $\langle \tau \rangle \sim N$  (log scale) for  $\Delta f_{LR} = 1$  (black circles),  $2$  (red squares), and  $3$  (green diamonds). The straight lines in each case is a linear fit with slope  $1.5 \pm 0.02$ . The inset at the left is the corresponding plot of  $\Delta f_{LR} \langle \tau \rangle \sim N$ .

of the effective translocation exponent  $\alpha \approx 1.5$  for chain lengths  $N \sim 100 - 500$  is the same as observed in a biased SNP [31, 33, 41]. This is discussed in detail below.

The scaling ansatz for the MFPT of a fully flexible chain in the context of a SNP translocation is given by [16, 17]

$$\langle \tau \rangle \sim [AN^{1+\nu} + \eta_{pore}N] |\Delta f_{LR}|^{-1} \sim N^\alpha. \quad (11)$$

Here  $A$  is constant,  $\nu = 0.75$  and  $0.5888$  is the Flory exponent in 2D and 3D, respectively, and  $\eta_{pore}$  is the pore friction. Eqn. 11 for a self-avoiding fully flexible chain holds for small to strong stretching force limits (trumpet, stem-flower, and strongly stretched) regimes [16, 17].

Following Cantor and Kardar, the origin of the first term is  $\langle \tau \rangle \sim \langle R_g \rangle / v_{CM} = N^\nu / N = N^{1+\nu}$  [38], where  $\langle R_g \rangle$  is the radius of gyration of the chain. The second term  $\eta_{pore}N$  in Eqn. 11 is the contribution of the pore friction  $\eta_{pore}$  and proportional to the contour length of the chain. When the chain length is small, then the pore friction term has a significant effect on the effective translocation exponent  $\alpha$  and  $1 < \alpha < 1+\nu$  [31, 33]. This is the reason for the smaller value of the effective translocation exponent  $1.5$  for the range of  $100 < N < 500$  rather than the  $\alpha = 1 + \nu = 1.75$  (2D). In the long

chain limit  $\alpha \rightarrow 1 + \nu$ , as the dominant contribution to the translocation time comes from the friction due to the movement of the polymer inside the solvent.

When the chain persistent length  $\ell_p \ll L$ , the Flory theory for the radius of gyration following Nakanishi [39] and Schaeffer, Pincus and Joanny [40] is written as

$$\sqrt{\langle R_g^2 \rangle} \sim \ell_p^{1/d+2} N^\nu. \quad (12)$$

In a previous paper we have shown the regime of  $L/\ell_p$  where the above relation is strictly valid [26]. Thus, in the limit when  $\ell_p \ll L$ , a plausible generalization of the scaling ansatz of Eqn. 11 is

$$\langle \tau \rangle \sim [A' \ell_p^{1/d+2} N^{1+\nu} + \tilde{\eta}_{pore}(\ell_p)N] |\Delta f_{LR}|^{-1} \sim N^\alpha. \quad (13)$$

The second term  $\tilde{\eta}_{pore}(\ell_p)$  is now is a function of the chain persistence length. Thus for a given persistence length  $\ell_p$ , Eqn. 13 reduces to Eqn. 11 with  $A = \ell_p^{1/d+2} A'$ , which then can be used to predict the behavior of longer semiflexible chains for the cases when  $\ell_p \ll L$ . The MFPT for shorter chains (still for those chain lengths for which  $L/\ell_p \gg 1$ ) are used to numerically obtain  $A$  and  $\eta_{pore}(\ell_p)$ , which then can be substituted in to Eqn. 11 to predict the MFPT of longer chains. This scheme is shown in Fig. 7. Eqn. 11 can be rewritten as follows:

$$\frac{\langle \tau \rangle |\Delta f_{LR}|}{N} = AN^\nu + \eta_{pore}(\ell_p) \quad (14)$$

Thus for a given value of the chain persistence length  $\ell_p$ , a plot of  $\langle \tau \rangle |\Delta f_{LR}| / N$  as a function of  $N^\nu$  will produce a straight line with the slope  $A$  and  $\eta_{pore}$  as the intercept. Fig. 7(a) clearly shows the validity of the scaling ansatz as in Eqn. 11. Here we have used Eqn. 13 and the simulation data for the MFPT for chain lengths  $N = 128, 192, 256$ , and  $320$  to obtain the value of the pore friction  $\tilde{\eta}_{pore}$  for  $\kappa = 8.0$  (the corresponding  $\ell_p = 2\kappa/k_B T = 13.3$ ). The choice of these chain lengths satisfy  $2.2 < L/\ell_p < 3.2$ , and from our previous work [26] we confirm that these combinations of  $L$  and  $\ell_p$  are well in the two dimensional self-avoiding random walk (2DSAW) regime and satisfy Eqn. 12. A linear regression perfectly fits the simulation data and that the data for different values of the bias  $|\Delta f_{LR}| = 2$  and  $3$  collapse on the same master plot with  $A = 0.219$  and  $\eta_{pore} = 6.929$ . Substituting these values of  $A$  and  $\eta_{pore}$  into Eqn. 11 ( $\langle \tau \rangle |\Delta f_{LR}| / N = 0.219 N^\nu + 6.929$ ) we extrapolate (dashed green line in Fig. 7(a)) to predict the MFPT for  $N = 384$  (brown star) and check that this point falls on top of the simulation data for  $N = 384$  (black circles and red squares). Once  $\eta_{pore}$  is known, one can also check that subtracting the pore friction contribution from  $\langle \tau \rangle$  provides a slope of  $1 + \nu$ . This is shown in Fig. 7(b) where a log-log plot of  $\langle \tau \rangle |\Delta f_{LR}| - \eta_{pore}N$  versus  $N$  indeed produces a slope  $\approx 1 + \nu$  (the regression produces a slope  $1.75 \pm 0.01$ ). This proves that in the limit  $d_{LR}/L \ll 1$  the scaling ansatz for the SNP translocation works for the model DNP system.

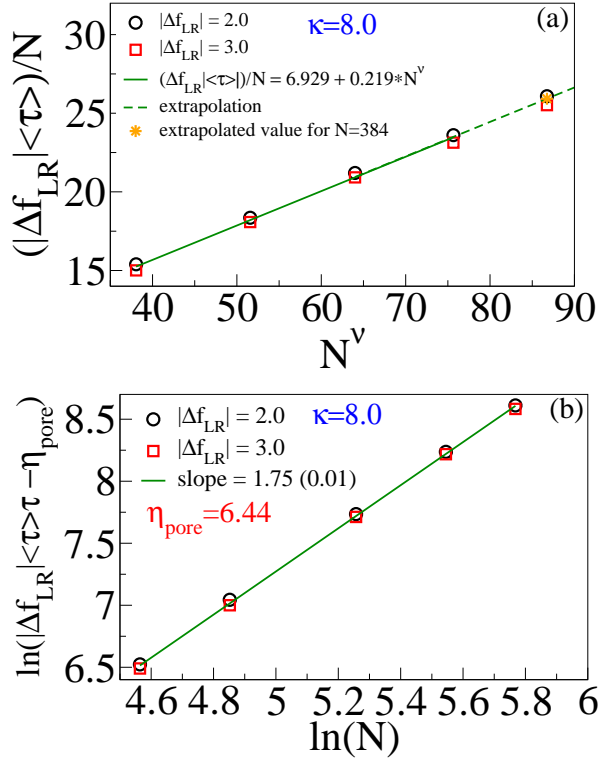


FIG. 7: (a) Plot of  $\langle \tau \rangle |\Delta f_{LR}|/N$  as a function of  $N^\nu$  for  $|\Delta f_{LR}| = 2$  (black circles) and 3 (red squares). The green solid line is a straight line fit through the points (which are average of black circles and red squares for each value of  $N = 128, 192, 256$ , and 320 respectively) enables us to determine  $A = 0.219$  and  $\eta_{pore} = 6.929$ . The brown star corresponds to the predicted value for  $N = 384$  from the extrapolated line (green dashed line), while the black circle and red square are the data obtained from simulation. (b) Demonstration that subtracting the pore friction one regains the asymptotic exponent of  $1 + \nu \approx 1.75 \pm 0.01$  for long chains.

It is worth noting that generalizing the scaling ansatz in three dimensions (3D) will be more challenging as unlike in 2D where the Gaussian regime is absent [26], the self-avoiding random walk (SAW) in 3D (3DSAW) appears at the end of the Gaussian regime and hence will require much longer chain lengths. Additionally, it is worth investigating the scaling ansatz for different regimes (rod, Gaussian and SAW) and for larger biases when the additional friction from the translocated segment of the chain may need to be incorporated separately [18].

#### IV. SUMMARY AND CONCLUSION

To conclude, we have studied various aspects of translocation in a model DNP system. The system we have studied is an ideal system motivated by recent

experiments to answer some general characteristics of translocation through a DNP in the limit  $d_{LR}/L \ll 1$ . Our studies of the TOW shows that the effect of the magnitude of the TOW forces will be more prominent for a ssDNA but likely to be insignificant for long dsDNA segments used in recent experiments. These conclusions were verified by studying the translocation of a triblock copolymer ABA and using the known result that a stiffer polymer translocates slower through a SNP. One of the primary motivation of recent experiments is to measure the current blockade time (TOF) for a tagged DNA segment of known length translocating through a DNP system. If the segment moves through the DNP with a constant velocity, then the current blockade time can be readily translated to the corresponding genomic length. Thus our studies of TOF is directly relevant for DNP experiments where the goal is to extract genomic distances from the data obtained in the time domain. We demonstrate that the TOF has a quasi-periodic structure, (implicating *non-uniform speed*). In the limit when  $d_{LR} \ll L$  by applying a net bias on the DNP we demonstrate that we recover scaling laws of SNP translocation. When  $d_{LR}/L \ll 1$  and the chain is subject to TOW forces, the entropic contribution from the segment in between the pore is almost insignificant compared to the total entropy of the chain. Thus, in this limit the pore friction term  $\eta_{pore}N$  from each pore adds up linearly (so that for the case of pores of same width it will simply be proportional to the number of pores), and one recovers the scaling ansatz for the SNP translocation. A DNP is an interesting system where one can create different chain conformations with variable tension and stiffness for the chain segment in between the pores by adjusting  $\tilde{f}_L$ ,  $\tilde{f}_R$ , and  $d_{LR}$ . Thus simulation studies of block copolymers and random heteropolymer translocation through DNP systems can produce intriguing and exciting results for studying nonlinear elasticity of biopolymers [42–44]. We hope that these results will provide further insights to design new experiments, be useful for making a theoretical framework for multi-pore translocation, and promote further work in this direction.

#### V. ACKNOWLEDGMENT

The authors acknowledge computing resources under the auspices of UCF's high performance computing cluster STOKES where all the computations were done. AB thanks Profs. Kurt Binder and Walter Reisner for various discussion and comments on the manuscripts. The authors gratefully acknowledge and thank both the referees for their comments and critiques on the manuscript.

- 
- [1] B. M. Venkatesan and R. Bashir, *Nature Nanotechnology* **6**, 615624 (2011).
- [2] For recent reviews in the field please see M. Muthukumar *Polymer Translocation* (CRC Press, Boca Raton, 2011); A. Milchev, *J. Phys. Condens. Matter* **23**, 103101 (2011); D. Panja, *J. Stat. Mech.* P06011 (2010); Vladimir V. Palyulin, Tapio Ala-Nissila, and Ralf Metzler, *Soft Matter*, **10**, 9016 (2014).
- [3] J. J. Kasianowicz, E. Brandin, D. Branton and D. W. Deamer, *Proc. Natl. Acad. Sci. U.S.A.* **93**, 13770 (1996).
- [4] A. Meller, L. Nivon, E. Brandin, J. A. Golovchenko, and D. Branton, *Proc. Natl. Acad. Sci. U.S.A.* **97**, 1079 (2000).
- [5] A. Meller, L. Nivon, and D. Branton, *Phys. Rev. Lett.* **86**, 3435 (2001).
- [6] A. Meller and D. Branton, *Electrophoresis* **23**, 2583 (2002).
- [7] S. Pud, S. Chao, M. Belkin, D. Verschueren, T. Huijben, C. van Engelenburg, C. Dekker, and A. Aksimentiev, *Nano Lett.* **16**, 8021 (2016).
- [8] Y. Zhang, X. Liu, Y. Zhao, J. -K. Yu, W. Reisner, and W. B. Dunbar, *Small* **14**, 1801890 (2018).
- [9] X. Liu, Y. Zhang, R. Nagel, W. Reisner, W. B. Dunbar, *Small* **15**, 1901704 (2019).
- [10] X. Liu, P. Zimny, Y. Zhang, A. Rana, R. Nagel, W. Reisner, and W. B. Dunbar, *Small* **16**, 1905379 (2020).
- [11] M. Langecker, *Nano Lett.* **11**, 5002 (2011).
- [12] Paolo Cadinu *et al.* *Nano Lett.* **17**, 6376 (2017).
- [13] Paolo Cadinu *et al.* *Nano Lett.* **18**, 2738 (2018).
- [14] K. Briggs *et al.*, *Nano Lett.* **18**, 660 (2018).
- [15] Jia-Wei Yeh, *Nano Lett.* **12**, 1597 (2012).
- [16] Ikonen T, Bhattacharya A, Ala-Nissila T, and Sung W *EPL* **103** 38001 (2013).
- [17] Ikonen T, Bhattacharya A., Ala-Nissila T. and Sung W. *J. Chem. Phys.* **137** 085101 (2012).
- [18] J. Sarabadoni, T. Ikonen, H. Mökkököken, T. Ala-Nissila, S. Carson, M. Wanunu, *Sci. Rep.* **7**, 7423 (2017).
- [19] T. Ikonen, A. Bhattacharya, T. Ala-Nissila and W. Sung, *Phys. Rev. E* **85**, 051803 (2012).
- [20] T. Sakaue, *Phys. Rev. E* **76** 021803 (2007); *ibid* **81**, 040808 (2010); T. Saito and T. Sakaue, *Eur. Phys. J. E* **34**, 135 (2011).
- [21] Adhikari R. and Bhattacharya A. *J. Chem. Phys.* **138**, 204909 (2013).
- [22] G. S. Grest and K. Kremer, *Phys. Rev. A* **1986**, 33, 3628(R) (1986).
- [23] A. D. Sokal, in *Monte Carlo and Molecular Dynamics Simulations in Polymer Science*, edited by K. Binder (Oxford University Press, New York, 1995), Chap. 2
- [24] A. Huang, R. Adhikari, A. Bhattacharya, and K. Binder, *Europhys. Lett.* **105**, 18002 (2014).
- [25] A. Huang and A. Bhattacharya, *Europhys. Lett.* **106**, 18004 (2014).
- [26] A. Huang, A. Bhattacharya, and K. Binder, *J. Chem. Phys.* **140**, 214902 (2014).
- [27] A. Huang, H.-P. Hsu, A. Bhattacharya, and K. Binder, *J. Chem. Phys.* **143**, 243102 (2015).
- [28] A. Huang, W. Reisner, and A. Bhattacharya, *Polymers* **8**, 352 (2016).
- [29] S. Bernier S, A. Huang, W. Reisner, and A. Bhattacharya, *Macromolecules* **51**, 4012 (2018).
- [30] K. Luo, T. Ala-Nissila, S. -C. Ying, and A. Bhattacharya, *Phys. Rev. Lett.* **99**, 148102 (2007); *ibid.* **100**, 058101 (2008).
- [31] A. Bhattacharya, W.H. Morrison, K. Luo, T. Ala-Nissila, S. -C. Ying, A. Milchev and K. Binder, *Eur. Phys. J. E* **29**, 423-429 (2009).
- [32] A. Bhattacharya and K. Binder, *Phys. Rev. E* **81**, 041804 (2010).
- [33] A. Bhattacharya, *Computer Simulation Studies in Condensed Matter Physics XXII*, Eds. D. P. Landau, S. P. Lewis, and H. B. Schuttler, Elsevier, *Physics Proceedings* **3**, 1411 (2010).
- [34] L. D. Landau and E. M. Lifshitz, *Statistical Physics*, Part 1, 3rd ed. (Pergamon Press, 1980).
- [35] van Gunsteren, W. F.; Berendsen, H. J. C. *Mol. Phys.* **1982**, 45, 637.
- [36] M. P. Allen and D. J. Tildesley, *Computer Simulation of Liquids* (Oxford University Press, Oxford, 1987).
- [37] M. Rubinstein and Ralph H. Colby, *Polymer Physics*, (Oxford University Press, 2003).
- [38] Y. Kantor and M. Kardar, *Phys. Rev. E* **69**, 021806 (2004).
- [39] H. Nakanishi, *J. Phys.* **48**, 979 (1987); J. Moon and H. Nakanishi, *Phys. Rev. A* **44**, 6427 (1991).
- [40] D. W. Schaefer, J. F. Joanny, and P. Pincus, *Macromolecules* **13**, 1280 (1980).
- [41] K. Luo, S. Ollila, I. Huopaniemi, T. Ala-Nissila, P. Pomorski, M. Karttunen, S-C. Ying, and A. Bhattacharya, *Phys. Rev. E* **78**, 050901(R) (2008).
- [42] Cornelis Storm, Jennifer J. Pastore, F. C. MacKintosh, T. C. Lubensky, & Paul A. Janmay, *Nature* **435**, 191 (2005).
- [43] Andrey V. Dobrynin and Jan-Michael Y. Carrillo, *Macromolecules* **44**, 140 (2011).
- [44] Jan-Michael Y. Carrillo, Fred C. MacKintosh, and Andrey V. Dobrynin, *Macromolecules* **46**, 3679 (2013).